The Canadian Mineralogist
Vol. 47, pp. 63-80 (2009)
DOI: 10.3749/canmin.47.1.63

CHROMIAN SPINEL IN THE TURNAGAIN ALASKAN-TYPE ULTRAMAFIC INTRUSION, NORTHERN BRITISH COLUMBIA, CANADA

J. Erik SCHEEL and James S. SCOATES[§]

Department of Earth and Ocean Sciences, University of British Columbia, 6339 Stores Road, Vancouver, British Columbia V6T 1Z4, Canada

Graham T. NIXON

British Columbia Geological Survey, Ministry of Energy, Mines and Petroleum Resources, PO Box 9333 Stn Prov Gov't, Victoria, British Columbia V8W 9N3, Canada

Abstract

The Early Jurassic Turnagain intrusion (24 km^2) in northern British Columbia, Canada, is one of a number of Alaskan-type intrusions that occur within the Mesozoic Quesnel accreted arc terrane. It is distinguished by the presence of magmatic Ni sulfide mineralization hosted by ultramafic cumulate rocks. Chromian spinel is a common accessory mineral (<0.5–4 vol.%) in the ultramafic rocks of the intrusion and is locally found as massive chromitite schlieren, pods, and rare layers in dunite. Although the composition of spinel from the Turnagain intrusion is highly variable, systematic compositional trends may be distinguished within individual samples and between samples from the different lithological units. Primary spinel compositions [$Fe^{3+}/(Fe^{3+} + Cr + Al) < 0.1$, $Cr/(Cr + Al) > 0.85$, $Fe^{2+}/(Fe^{2+} + Mg) < 0.4$] are preserved in magnesiochromite grains from the chromitites, which were isolated from nearby olivine and interstitial melt and thus did not significantly re-equilibrate during cooling. Extensive re-equilibration with evolved interstitial melt, defined by broadly linear trends of increasing Al, Fe^{3+}, Ti, V and $Fe^{2+}/(Fe^{2+} + Mg)$ with decreasing Cr content, is recorded in chromian spinel grains from dunite, wehrlite, and olivine clinopyroxenite. These trends converge toward the compositional field of grains from the chromitites. Rims of Fe^{3+}-rich chromite and Cr-bearing magnetite, up to 30 μm thick, formed around chromian spinel grains during subsolidus infiltration of oxygenated fluids and serpentinization. Relative to the global database of spinel compositions from Alaskan-type intrusions, the majority of the chromian spinel compositions from the Turnagain intrusion are characterized by lower $Fe^{3+}/(Fe^{3+} + Cr + Al)$ and higher $Cr/(Cr + Al)$, which is consistent with a relatively low oxygen fugacity for the parental magmas to the ultramafic cumulates. The Turnagain parental magmas were likely reduced by assimilation of graphite- and pyrite-bearing phyllite host-rocks, which led to local saturation in a sulfide liquid.

Keywords: Turnagain intrusion, Alaskan-type intrusion, chromian spinel, chromitite, ultramafic rocks, electron-microprobe analyses, re-equilibration, oxygen fugacity, British Columbia.

Sommaire

Le complexe intrusif de Turnagain (24 km^2), dans le nord de la Colombie-Britannique, Canada, d'âge jurassique précoce, est membre d'une association de massifs intrusifs de type Alaska dans le socle mésozoïque d'arcs accrétés de Quesnel. Il se distingue par la présence d'une minéralisation en sulfures magmatiques de Ni encaissée dans les cumulats ultramafiques. Le spinelle chromifère est un accessoire répandu dans les roches ultramafiques du complexe (<0.5–4% du volume), localement accumulé pour former des inclusions, lentilles et couches de chromitite dans la dunite. Quoique la composition du spinelle de l'intrusion Turnagain est très variable, on distingue des variations systématiques de la composition au sein d'échantillons individuels ou parmi les échantillons de différentes unités du complexe. Les compositions primaires [$Fe^{3+}/(Fe^{3+} + Cr + Al) < 0.1$, $Cr/(Cr + Al) > 0.85$, $Fe^{2+}/(Fe^{2+} + Mg) < 0.4$] sont préservées dans la magnésiochromite des chromitites, qui étaient isolées par rapport à l'olivine et le liquide silicaté adjacent, et donc qui n'ont pas ré-équilibré de façon importante au cours du refroidissement. On reconnait les effets d'un ré-équilibrage plus répandu avec le bain fondu interstitiel, tel que défini par des variations plus ou moins linéaires montrant une augmentation en Al, Fe^{3+}, Ti, V et $Fe^{2+}/(Fe^{2+} + Mg)$ à mesure que diminue la teneur en Cr, dans le spinelle chromifère de la dunite, wehrlite, et clinopyroxénite à olivine. Ces tendances convergent vers le champ de compositions typiques des échantillons de chromitite. Des liserés de chromite enrichie en Fe^{3+} et de magnétite chromifère, atteignant 30 μm en épaisseur, se sont formés autour des grains de spinelle chromifère au cours de l'infiltration de fluide oxygéné et de la serpen-

§ *E-mail address*: jscoates@eos.ubc.ca

tinisation. Par rapport aux données disponibles sur la composition des spinelles des intrusions de type Alaska, la majorité des compositions provenant du complexe intrusif de Turnagain ont des valeurs de $Fe^{3+}/(Fe^{3+} + Cr + Al)$ plus faibles et des valeurs de Cr/(Cr + Al) plus élevées, ce qui concorde avec une fugacité plus faible d'oxygène des venues de magma qui ont produit les cumulats ultramafiques. Ces venues seraient devenues réduites par assimilation de l'encaissant, des phyllites contenant graphite et pyrite, ce qui a mené à une saturation locale en liquide sulfuré.

(Traduit par la Rédaction)

Mots-clés: massif intrusif de Turnagain, complexe de type Alaska, spinelle chromifère, chromitite, roches ultramafiques, analyses avec microsonde électronique, ré-équilibrage, fugacité d'oxygène, Colombie-Britannique.

Introduction

Chromian spinel, found as an accessory mineral in a wide variety of mafic and ultramafic rocks, is typically one of the earliest phases to crystallize in basic–ultrabasic magmas (*e.g.,* Roeder 1994, Barnes 1998, Barnes & Roeder 2001). The abundance of chromian spinel in many mafic–ultramafic rocks is generally low (~1 vol.%), although accumulations form chromitite layers and pods in layered intrusions and ophiolites. Chromian spinel is also found associated with the least-evolved rock types of Alaskan-type intrusions. Alaskan-type intrusions are mafic–ultramafic complexes dominated by dunite, wehrlite, olivine clinopyroxenite, and clinopyroxenite, with chromian spinel present in the most Mg-rich rocks; the absence of orthopyroxene is a defining characteristic of Alaskan-type intrusions (Taylor 1967, Irvine 1974). Hornblende-bearing lithologies (hornblende clinopyroxenite, clinopyroxene hornblendite, hornblendite) and plagioclase-bearing rocks (gabbro, diorite) containing magnetite (± ilmenite) represent the more evolved portions of these intrusions. Alaskan-type intrusions also typically show a crude internal zonation of ultramafic and mafic lithologies, and, with the notable exception of Duke Island (Irvine 1974, 1987), igneous layering on the outcrop scale is rare.

The Barnes & Roeder (2001) compilation of spinel compositions from mafic–ultramafic rocks worldwide includes only seven referenced sources of data for Alaskan-type intrusions for a total of 386 individual spinel datasets. Although Garuti *et al*. (2003) and Krause *et al*. (2007) provided additional spinel composition from Uralian–Alaskan-type intrusions in the Ural Mountains, Alaskan-type intrusions form the most under-represented major category of igneous rocks with respect to spinel compositions in the global database. In this study, we present new analytical data on spinel-group phases from the Turnagain Alaskan-type intrusion in northwestern British Columbia, with the aim of 1) increasing the compositional database for spinel in Alaskan-type intrusions, 2) determining the sequence of crystallization in the intrusion and subsequent chemical modifications during cooling and serpentinization using the compositional variability of chromian spinel, and 3) assessing the relative redox conditions of the parental magmas for the Turnagain intrusion.

Regional Geology

Numerous Alaskan-type intrusions in British Columbia (B.C.) occur within the Mesozoic Quesnel accreted arc terrane, including the Tulameen (Findlay 1969), Polaris (Foster 1974), Lunar Creek, Wrede Creek, Johansson Lake (Nixon *et al*. 1997), and Turnagain (Clark 1975, 1978, 1980, Nixon 1998) intrusions. The Turnagain intrusion is located in northwestern B.C., approximately 70 km east of Dease Lake. It lies east of the Kutcho Fault, a regional strike–slip fault that delineates the terrane boundary between Ancestral North America to the north and Quesnellia to the south (Gabrielse 1998). The 24 km^2 Turnagain intrusion is fault-bounded; during the Early Jurassic, it was thrust onto graphitic and pyritic phyllites currently assigned to the undivided Ordovician–Devonian Road River Formation of the Earn Group, a deep marine facies of paleo-passive-margin sedimentary units of Ancestral North America (Gabrielse 1998). Conformably overlying the phyllite is a Devonian–Mississippian volcanic and sedimentary unit (Erdmer *et al*. 2005) that may be correlative with the Lay Range Assemblage (Scheel 2007). The age of crystallization of the Turnagain intrusion is constrained to be ~190 Ma on the basis of combined U–Pb and $^{40}Ar/^{39}Ar$ geochronological results (Scheel 2007).

Geology and Spinel Content of the Turnagain Intrusion

The Turnagain intrusion contains predominantly coarse-grained ultramafic cumulate rocks (dunite, wehrlite, olivine clinopyroxenite and hornblende clinopyroxenite) with associated late hornblende-bearing dioritic phases and intrusions (Clark 1980, Nixon 1998). The intrusion forms a northwest-trending elongate body (3.5 × 8.5 km) with an apparent thickness of approximately 450 m, as estimated from inverse modeling of gravity data (C. Baldys, pers. commun. 2005) (Fig. 1). Outcrop exposures are limited to the northern and northeastern parts of the intrusion, which are above the treeline, and near Ni-sulfide mineralized zones to the southeast near the Turnagain River (Fig. 1). Although fault-bounded, the intrusion is crudely zoned, with dunite in the north-central region, clinopyroxene-bearing lithologies to the southeast and northwest that

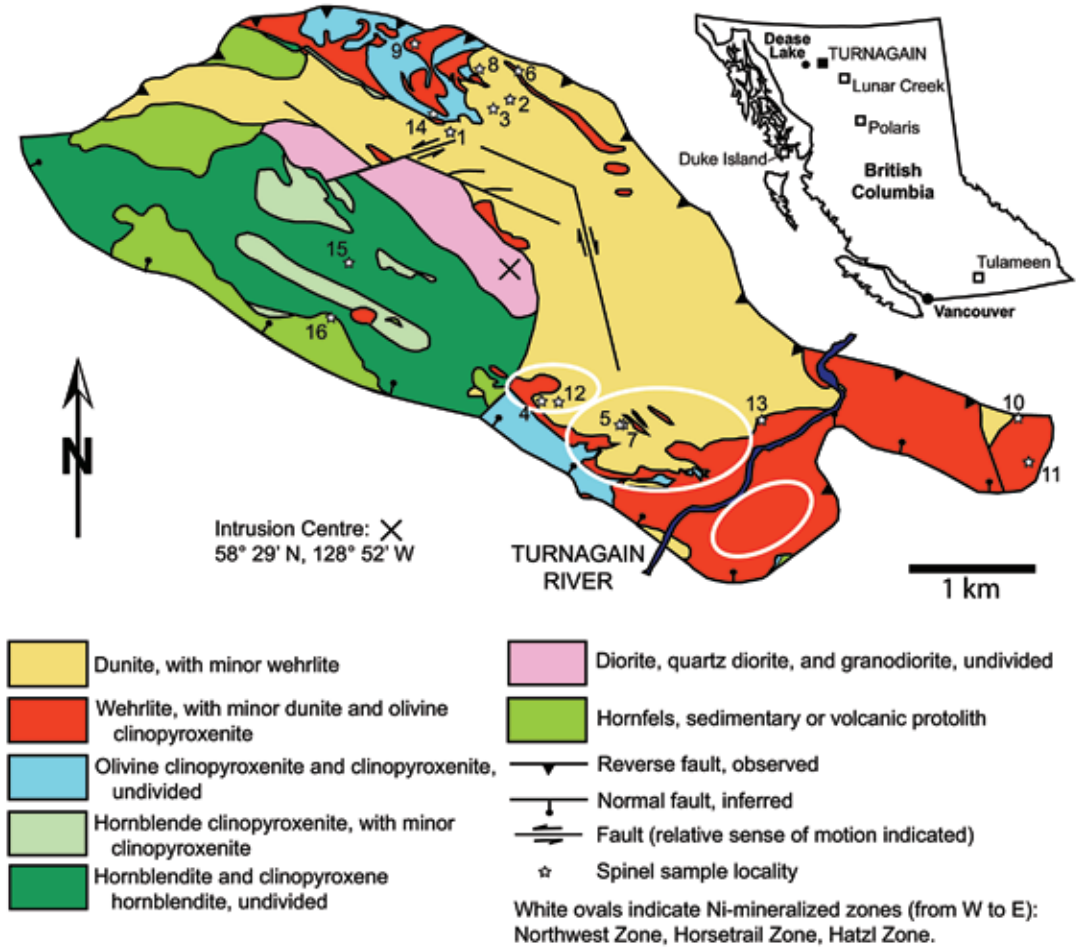

FIG. 1. Simplified geological map of the Turnagain Alaskan-type intrusion, modified from Clark (1975) and including new mapping results from this study. The location of the Turnagain intrusion (filled square) in British Columbia is shown as an inset in the upper right corner (also indicated are the locations of other major Alaskan-type intrusions in B.C. and Alaska, shown as open square symbols). The Ni sulfide mineralized zones (Horsetrail, Hatzl and Northwest zones) are outlined in white ovals in the southeastern part of the intrusions. Sample locations with spinel compositions discussed in this paper are indicated as white stars; the adjacent numbers refer to complete sample number and location (UTM coordinates) information provided in Appendix 1.

envelop the dunite, and a heterogeneous assemblage of hornblende-bearing rocks in the western part of the intrusion.

Primarily on the basis of rock types present and the absence of orthopyroxene, the Turnagain meets the requirements of an "Alaskan-type" intrusion (Nixon 1998). However, the Turnagain is an unusual Alaskan-type intrusion in that it contains significant Ni-sulfide mineralization, with measured and indicated resources of 428 Mt grading 0.17% sulfide Ni (Simpson 2007). Massive to semimassive Fe–Ni–Cu sulfide mineralization and broad zones of disseminated primary sulfide minerals are hosted by dunite and clinopyroxene-bearing intrusive phases (wehrlite, olivine clinopyroxenite) along the southern and eastern margins of the intrusion (Horsetrail, Hatzl and Northwest zones); dunite in the north-central part of the intrusion is essentially devoid of sulfide minerals. In order of decreasing abundance, primary sulfide minerals consist of pyrrhotite, pentlandite, minor chalcopyrite, and trace bornite. Textures in the mineralized zones range from interstitial to blebby sulfide minerals in the disseminated zones to net-textured, globular, and banded sulfide concentrations in the massive to semimassive mineralized zones

(Nixon 1998, Scheel 2007, Simpson 2007). Evidence for local remobilization of primary sulfide minerals includes the presence of pyrrhotite (+ chalcopyrite) along fractures and veins adjacent to serpentinized areas, dikes, and altered xenoliths, as well as the local presence of secondary sulfide minerals such as violarite and valleriite.

Within the Turnagain intrusion, chromian spinel is common in the cumulate rocks richest in magnesian olivine (dunite and wehrlite), whereas magnetite is typical of the more evolved, clinopyroxene- and hornblende-bearing lithologies that comprise the westernmost portion of the intrusion. The distribution of oxide minerals in the Turnagain intrusion was originally described by Clark (1978), who also analyzed chromian spinel by electron microprobe (nine core and six rim compositions). In the following section, the typical abundances and textures of spinel in rocks examined in this study are described prior to an evaluation of their compositional variations. The compositions of coexisting olivine (Fo_{ol}) and clinopyroxene ($Mg\#_{cpx}$) indicated below are reported in Scheel (2007), where they are used in a broader petrological and geochemical study of the crystallization history of the Turnagain intrusion.

Dunite and chromitite

Dunite, the most abundant rock-type in the Turnagain intrusion, contains cumulus olivine ($Fo_{89–92.5}$) and chromian spinel with minor interstitial clinopyroxene (<10 vol.%) and rare phlogopite (0–1 vol.%). Equigranular olivine (2 mm across) is typical of most samples of dunite. Incipient serpentinization of olivine is common, with the average extent of serpentinization being ~10 vol.%. Secondary fine-grained magnetite is common between olivine grains.

Chromian spinel in dunite occurs primarily as disseminated grains (~2 vol.%) and as sparsely distributed schlieren of chromitite (up to 30 cm long and several cm wide), pods, lamellae, and rare layers (<5 cm thick) (Fig. 2). The chromitite samples examined in this study were sampled from the northernmost exposures of dunite, in the alpine area near the margin of the exposed intrusion (Fig. 1). Grain sizes of spinel are typically largest in chromitite (up to 3 mm) and slightly smaller in dunite (up to 2 mm): grain shapes are predominantly equant in chromitite (Figs. 3A,B). The disseminated grains of spinel are typically euhedral (Fig. 3C) and occur as inclusions and along grain boundaries.

Secondary alteration of chromian spinel in dunite has resulted in the formation of overgrowths of magnetite (~30 μm thick) or ferrian chromite – magnetite solid solution (Fe^{3+}-rich chromite) (Fig. 3D). Chromian spinel grains within or partially encased by clinopyroxene typically do not show a secondary overgrowth or rim.

Wehrlite

Cumulus olivine ($Fo_{85–90}$) and interstitial (intercumulus) clinopyroxene are the dominant phases in wehrlite, although rare cumulus diopside does occur locally ($0.87 < Mg\#_{cpx} < 0.96$). The grain size of olivine is comparable to that in dunite (~2 mm); equigranular textures are less common and restricted to clinopyroxene-poor rocks; however, olivine contained, either partially or entirely, within large clinopyroxene oikocrysts is typically roundish. Where present, cumulus clinopyroxene is commonly finer-grained than neighboring olivine, with grain sizes ranging from 75 μm to 2 mm in diameter. Serpentine-group minerals replace only olivine in wehrlite, and secondary magnetite is common along grain boundaries.

Disseminated chromian spinel in wehrlite, typically ~150 μm in diameter, is less abundant than in dunite (Figs. 4A, B) and concentrated in clusters of euhedral grains. The majority of chromian spinel grains are included in olivine or lie along silicate grain-boundaries, or rarely enclosed by interstitial clinopyroxene. Both rims of magnetite and Fe^{3+}-rich chromite around chromian spinel are as common in wehrlite as in dunite.

Olivine clinopyroxenite

Olivine clinopyroxenite is typically composed of variable amounts of cumulus olivine ($Fo_{83–87}$) and clinopyroxene ($0.90 < Mg\# < 0.97$). Several samples contain abundant oikocrystic clinopyroxene; this textural type commonly contains more chromian spinel than olivine clinopyroxenite with cumulus textures. The grain size of olivine (~1 mm) is relatively small, whereas clinopyroxene grains may reach 15 mm across. Olivine-poor clinopyroxenite typically contains strongly serpentinized olivine.

Chromian spinel is mostly found as inclusions within cumulus clinopyroxene or olivine and rarely exhibits a rim of secondary magnetite (Figs. 4C, D). The grain size is typically small (~150 μm), and grains are commonly euhedral (Fig. 4D). The abundance of chromian spinel is low (<0.5 vol.%) compared to wehrlite and dunite; however, grain textures and size are similar.

Hornblende clinopyroxenite and hornblendite

Hornblende clinopyroxenite ($0.78 < Mg\#_{cpx} < 0.86$) and hornblendite occur in two distinct settings: 1) as fine-grained dikes considered to represent evolved compositions of magma (Scheel 2007), and 2) lithologies integral to the west-central part of the main intrusion, some of which exhibit cumulus textures. The latter lithologies typically contain primary magnetite, which is locally coarse-grained (up to 1 cm diameter), whereas hornblendite dikes, which intrude both ultramafic rocks and hornfelsed wallrocks, commonly contain subhedral

ilmenite. Magnetite commonly contains lamellae of ilmenite formed through oxy-exsolution.

Analytical Techniques

Samples selected for analysis from the main ultramafic rock units of the Turnagain intrusion (see Fig. 1 for sample locations, and Appendix 1 for UTM coordinates) represent the range of spinel morphologies and spinel–silicate associations described above. The spinel content of each sample, textural relationships to other phases, and degree of alteration were carefully scrutinized using both transmitted and reflected light microscopy. Local accumulations or "clusters" of spinel grains were observed in most samples. Spinel grains from three distinct clusters were analyzed in each thin section, and three spot analyses were done on each grain (core, mid-point, and rim).

A total of 16 samples were selected for electron-microprobe analysis, carbon-coated, and documented using a Philips XL–30 scanning electron microscope at the University of British Columbia, Vancouver, British Columbia. Quantitative analyses were carried out in wavelength-dispersion mode using a Cameca SX–50 electron microprobe with a beam diameter of 10 μm, an accelerating voltage of 15 kV, and a beam current of 20 nA, with 20 s peak count-time and 10 s background count-time. The Ni contents of chromian spinel grains from the chromitite samples were analyzed using a fixed matrix, a beam diameter of 10 μm, an accelerating voltage of 15 kV, and a beam current of 200 nA with peak count-time extended to 100 s and a background time to 50 s. For the elements considered, the following standards, X-ray lines and crystals were used: synthetic rhodonite: Mn*K*α, LIF; diopside: Ca*K*α, PET, and Si*K*α, TAP; synthetic spinel: Al*K*α, TAP; synthetic fayalite, Fe*K*α, LIF; synthetic magnesiochromite: Mg*K*α, TAP, and Cr*K*α, LIF; rutile: Ti*K*α, PET; V metal: V*K*α, PET; synthetic Ni_2SiO_4: Ni*K*α, LIF. Data reduction of all analytical results was undertaken using the "PAP" $\phi(\rho Z)$ procedure of Pouchou & Pichoir (1985). Using the higher beam-current and counting times for Ni as described above yields an analytical precision of <5% relative. We analyzed spinel at a total of 360 points, 25 of which correspond to magnetite. All spinel compositions were assumed to be stoichiometric (Kamperman *et al*. 1996); cation abundances and the ratio of ferrous to ferric iron were calculated using the method of Barnes & Roeder (2001).

Results

Table 1 contains representative compositions of spinel grains from the various ultramafic lithologies of the Turnagain intrusion. The complete set of data obtained in this study is available as an electronic supplement (Table A1), available from the Depository of Unpublished Data, on the MAC website [document Turnagain CM47_63]. The variations in spinel compositions are described below for each of the major rock types and plotted in Figures 5–8.

Chromitite

Spinel grains from the chromitites are predominantly magnesiochromite and are characterized by the most Cr- and Mg-rich compositions of all lithologies ($59 < Cr_2O_3 < 67$ wt.%, $10 < MgO < 14$ wt.%) with correspondingly low TiO_2 (0.24–0.66 wt.%), V_2O_3 (0.01–0.34 wt.%), Al_2O_3 (4.60–7.14 wt.%), and Fe_2O_3 (3.82–6.88 wt.%) contents (Figs. 5–8). Two samples (05ES–01–03–01 and 05ES–01–04–01) contain relatively Ni-rich chromite grains ($0.13 < NiO < 0.20$ wt.%). All spinel compositions in chromitite are distinguished by $Fe^{3+}/(Fe^{3+} + Cr + Al) < 0.1$ (Figs. 5–8). Systematic zoning in the magnesiochromite grains is not evident.

Dunite

Compositions of the chromian spinel from dunite span a relatively large interval ($34 < Cr_2O_3 < 56$ wt.%, $0.01 < TiO_2 < 1.01$ wt.%, $20 < FeO < 29$ wt.%, $3.5 < Fe_2O_3 < 18.6$ wt.%) compared to those from the chromitites (Figs. 5, 6). With the exception of sample 04ES–19–01–02, the compositions from each sample of dunite, and zoning within individual grains, show an overall iron-enrichment trend (Fig. 6A), which is a common feature of Alaskan-type intrusions (Barnes & Roeder 2001). All Fe^{3+}-rich spinel compositions in dunite with $Fe^{3+}/(Fe^{3+} + Cr + Al) > 0.35$ represent Fe^{3+}-rich chromite or Cr-bearing magnetite developed as a rim on chromian spinel grains. Such rims are intimately associated with serpentine-group minerals. Compositions from sample 04ES–19–01–02 have $Fe^{3+}/(Fe^{3+} + Cr + Al)$ less then 0.1, values similar to those from the chromitites.

Wehrlite

Compositions of chromian spinel from wehrlite show a wide compositional range and are relatively enriched in Al (7.5–15.4 wt.% Al_2O_3), Ti (0.7–1.8 wt.% TiO_2) and Fe (10–18 wt.% Fe_2O_3) (Figs. 5–8). The presence of Cr-bearing magnetite and Fe^{3+}-rich chromite rims, albeit rare, indicates that similar processes of secondary alteration affected both wehrlite and dunite. Compositions from one wehrlite sample (04ES–15–01–05) have markedly lower $Fe^{3+}/(Fe^{3+} + Cr + Al)$ values compared to other samples of wehrlite (Figs. 5–8). The spinel grains in this sample are unzoned, with the lowest Fe_2O_3 contents (0.94–3.97 wt.%) of all data gathered here, and relatively low Cr/(Cr + Al) (0.68–0.73), high Ti (1.1–2.5 wt.% TiO_2), and high V (0.06–0.38 wt.% V_2O_3). In terms of their abundances of trivalent cations

(Fig. 5A), compositions of chromian spinel from individual wehrlite samples and zoning within individual grains, with the exception of 04ES–15–01–05, are characterized by intermediate sloping trends (*i.e.,* decreasing Cr, increasing Fe^{3+} and Al).

Olivine clinopyroxenite

Most samples of olivine clinopyroxenite in the Turnagain intrusion, and indeed in other Alaskan-type intrusions (Irvine 1965), are devoid of chromian spinel. Rare spinel grains from olivine clinopyroxenite are relatively enriched in FeO (23–27 wt.%), Fe_2O_3 (9.7–17.2 wt.%), Ti (0.9–2.1 wt.% TiO_2) and V (0.22–0.54 wt.% V_2O_3), and depleted in Al (5.68–9.40 wt.% Al_2O_3) compared to spinel from the other rock types. One notable exception is sample 04ES–01–04–01, which contains chromian spinel grains with $Fe^{3+}/(Fe^{3+} + Cr + Al)$ less than 0.1 (Figs. 5–8) and which overlaps with the compositions from dunite sample 04ES–19–01–02. Compositions from sample 05ES–05–01–01 are also distinctive, with high amounts of Ti (2.5–3.2 wt.% TiO_2) and $Fe^{3+}/(Fe^{3+} + Cr + Al)$ greater than 0.4. All analyzed grains (cores and rims) from this sample are Fe^{3+}-rich chromite. With respect to trivalent cations, the chromian spinel grains from olivine clinopyroxenite do not show the strong within-sample variations that are observed in the dunites and wehrlites.

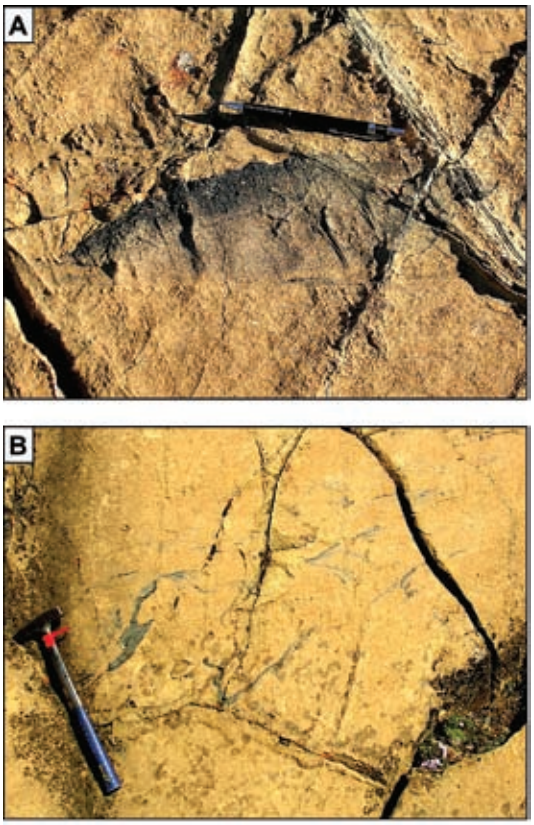

FIG. 2. Photographs of chromitite in outcrop from the north-central portion of the Turnagain intrusion. A) Chromitite schlieren grading into dunite toward the lower part of the photograph. Cross-cutting veins are filled with serpentine-group minerals. Pencil is approximately 12 cm long. B) Numerous schlieren of chromitite, which may represent disrupted layers, within dunite. Hammer is approximately 50 cm long.

Hornblende clinopyroxenite

The spinel from two magnetite-bearing hornblende clinopyroxenites, both from drillcore, show contrasting compositions. The analyses from sample DDH05–84–19 indicate nearly pure end-member magnetite ($67.1 < Fe_2O_3 < 67.8$ wt.%, $0.37 < Cr_2O_3 < 0.60$ wt.%, and Al in the range 0.06–0.18 wt.% Al_2O_3), whereas spinel from sample DDH04–47–49 shows slight Al-enrichment (Al_2O_3 in the range 0.12–3.77 wt.%) and relative enrichment in V (V_2O_3 in the range 0.22–0.73 wt.%), and exhibits high Ti (0.15–4.0 wt.% TiO_2) (Fig. 7). Magnetite crystals in hornblende clinopyroxenite are distinguished from the magnetite rims on chromian spinel grains in dunite, wehrlite, and olivine clinopyroxenite by the lack of Cr and the presence of small amounts of Al (Fig. 5A). There is no systematic zoning observed in the magnetite grains analyzed.

DISCUSSION

The composition of chromian spinel has long been recognized as a powerful petrogenetic indicator in petrological studies (*e.g.,* Irvine 1965, 1967, Dick & Bullen 1984, Roeder & Campbell 1985, Sack & Ghiorso 1991, Scowen *et al.* 1991, Power *et al.* 2000 , Poustovetov & Roeder 2001, Kamenetsky *et al.* 2001) and in investigations of ore-forming processes in komatiites (Barnes 1998, Barnes & Brand 1999, Fiorentini *et al.* 2008). Compositional variations in chromian spinel may record changes in magma composition and the nature of coprecipitating phases (Roeder 1994), oxygen fugacity (*e.g.,* Poustovetov & Roeder 2001) and pressure (*e.g.,* Roeder & Reynolds 1991). The composition of primary spinel grains may also be modified by synmagmatic and postmagmatic processes (*e.g.,* Roeder & Campbell 1985, Power *et al.* 2000). In particular, re-equilibration with interstitial melt or silicate mineral hosts and serpentinization may change the composition of spinel (*e.g.,* Roeder & Campbell 1985, Sack & Ghiorso 1991, Scowen *et al.* 1991, Roeder 1994, Mellini *et al.* 2005). The significance of compositional variability in spinel of the Turnagain Alaskan-type intrusion is addressed below.

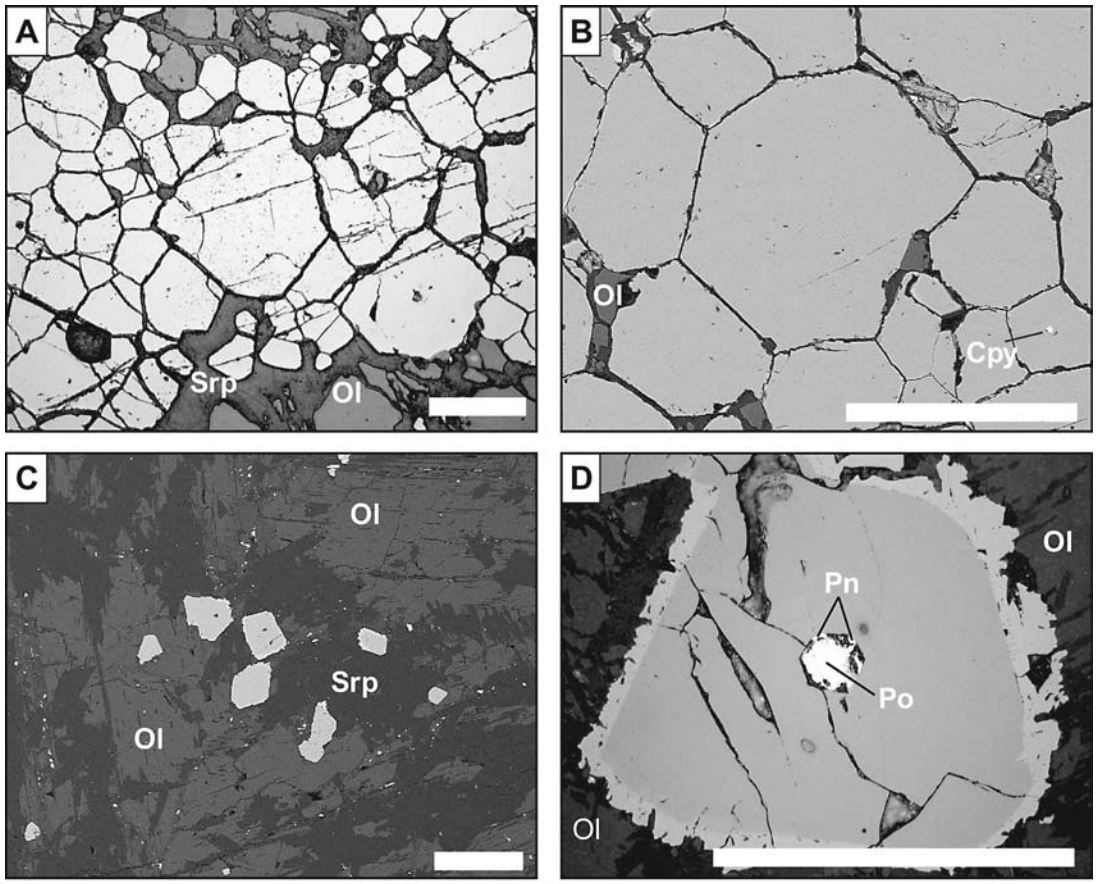

FIG. 3. Photomicrographs of chromian spinel textures from chromitite and dunite in the Turnagain intrusion. The white scale-bar on each photo is 200 μm in length. A) Reflected light, sample 05ES–01–01–01, cluster 5. Polygonal grains of magnesiochromite of variable size occur within a thin seam of chromitite enclosed in dunite consisting of olivine (Ol) and secondary serpentine (Srp) after olivine. B) BSE (back-scattered electron) image, sample 05ES–01–01–01, cluster 4. Massive chromitite showing equigranular grain-shapes and 120° grain-boundary junctions produced during slow cooling and recrystallization. A small inclusion of chalcopyrite (Cpy) is found in a magnesiochromite grain in the bottom right of the photograph. C) BSE image, sample 04ES–10–05–01, cluster 2. This cluster, within a partially serpentinized dunite, shows the primary euhedral nature of the chromite grains as well as the initial development of a thin rim of magnetite (bright material on edge of grains). D) Reflected light, sample 04ES–08–01–01. Single grain of chromite with a sulfide inclusion. The inclusion originally consisted of an immiscible sulfide liquid that crystallized to pyrrhotite (Po) and pentlandite (Pn); note that the habit of the sulfide inclusion was determined by its host chromite grain. The distinctly brighter and irregular rim around the chromite grain is Fe^{3+}-rich chromite produced during serpentinization.

Compositions of primary spinel

Chromian spinel grains from chromitite schlieren, wisps, pods, and layers have the most Cr-rich, Al- and Fe^{3+}-poor, and lowest $Fe^{2+}/(Fe^{2+} + Mg)$ compositions in the Turnagain intrusion (Figs. 5–8), especially samples 05ES–01–04–01 and 05ES–01–03–01 (indicated as group 1 in Fig. 7A and 8A). They are also characterized by relatively low $Fe^{3+}/(Fe^{2+} + Fe^{3+})$, in the range 0.23–0.32 (Fig. 5B). These grains may preserve primary (*e.g.,* 05ES–01–04–01) or near-primary spinel compositions, which occurred because the magnesiochromite grains in the chromitites were effectively isolated from interstitial melt and nearby olivine, thus preventing both subliquidus re-equilibration with residual liquid and subsolidus re-equilibration with enclosing silicates, respectively. These grains record the least evolved

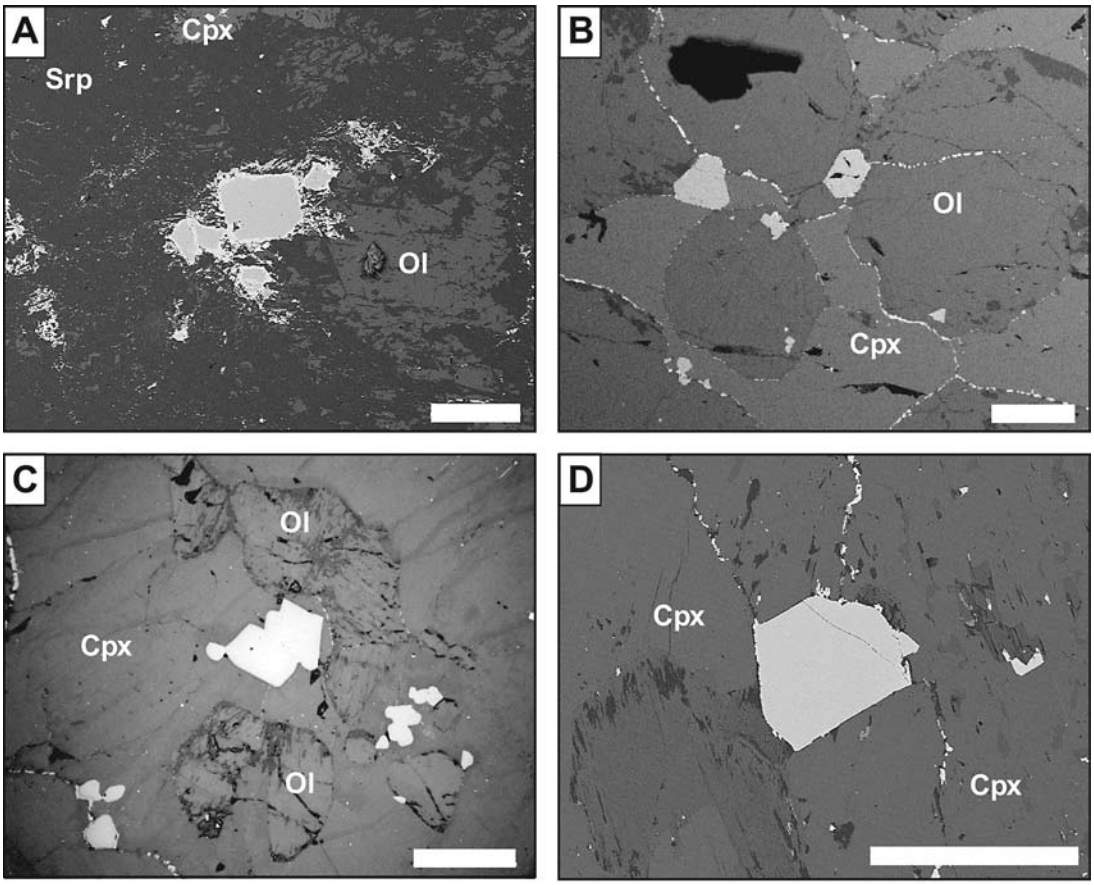

FIG. 4. Photomicrographs of chromian spinel textures from wehrlite and olivine clinopyroxenite in the Turnagain intrusion. The scale bar on each photo is 200 μm in length. A) BSE image, sample 04ES–10–06–01, cluster 5. This strongly serpentinized wehrlite contains only a few grains of chromian spinel, and those present show a well-developed magnetite – Fe^{3+}-rich chromite rim, as well as a distinct aureole of magnetite (localized, very fine-grained magnetite). B) BSE image, sample 04ES–15–01–05, cluster 1. Small, euhedral grains of chromian spinel between cumulus olivine grains with little to no magnetite rim. Note the presence of fine-grained magnetite along grain boundaries between cumulus minerals and within fractures. C) Reflected light, sample 04ES–01–04–01, cluster 5. Euhedral grains of chromian spinel in olivine clinopyroxenite with cumulus olivine and abundant interstitial clinopyroxene. D) BSE image, sample 05ES–05–01–01, cluster 7. One of only two chromian spinel grains found in the entire thin section; this grain is entirely encased within cumulus clinopyroxene.

spinel compositions; they crystallized from the most primitive (highest-Mg) magmas.

Fractionation and re-equilibration trends

Grains of chromian spinel in the chromitite samples 05ES–01–04–01 and 05ES–01–03–01 show a weak compositional trend characterized by slightly increasing $Fe^{2+}/(Fe^{2+} + Mg)$ at near-constant $Fe^{3+}/(Fe^{3+} + Cr + Al)$ and $Cr/(Cr + Al)$ (Figs. 5, 6, 8). This change in composition is consistent with the effect of olivine (Mg-rich) + spinel (Fe^{2+}-dominant) fractionation as temperature decreased (*e.g.*, Roeder *et al.* 2001). Such subtle compositional changes may have occurred prior to emplacement in a melt-dominant environment during transport within ascending Turnagain magmas.

All other chromian spinel grains, including those from the chromitite sample 05ES–01–01–01 that represents a 2 mm-thick chromitite seam, have undergone compositional modification at high temperatures during interaction with evolved interstitial melt, enclosing silicates, or an oxygenated fluid. The chromian spinel compositions from many of the individual samples of dunite, wehrlite and olivine clinopyroxenite define

broadly linear trends with intermediate slopes in the Fe^{3+}–Cr–Al plot (*i.e.,* higher relative Al and Fe^{3+} with decreasing Cr; trend 2 in Fig. 8A), which also correlate with increasing $Fe^{2+}/(Fe^{2+} + Mg)$, Ti and V (Figs. 6, 7). The grains within these trends span a range of $Fe^{3+}/(Fe^{2+} + Fe^{3+})$ from 0.25 to 0.40 (Fig. 5B). These trends converge toward the Cr apex of the Fe^{3+}–Cr–Al diagram, toward the compositional field for spinel from chromitites. These converging trends could be explained by re-equilibration of original primary or near-primary chromite with evolved, interstitial melt, which would have been relatively enriched in Ca, Al, Ti, and Fe^{3+}, during progressive consolidation of these cumulate rocks. Fractionated interstitial melt would have been in direct contact with those spinel grains along silicate grain-boundaries, thus facilitating re-equilibration, or diffusive exchange may have occurred through olivine for olivine-hosted spinel grains (*e.g.,* Roeder & Campbell 1985).

The unusual compositions of spinel from wehrlite sample 04ES–15–01–05 and olivine clinopyroxenite sample 04ES–01–04–01, with their relatively low Cr/(Cr + Al) and $Fe^{3+}/(Fe^{3+} + Cr + Al)$ values less than 0.1 (trend 3 in Fig. 8A), combined with very low $Fe^{3+}/(Fe^{2+} + Fe^{3+})$ values (less than 0.18) (Fig. 5B), may have resulted from re-equilibration with clinopyroxene. Both samples contain cumulus olivine and chromite grains enveloped by clinopyroxene oikocrysts 2 cm in diamter, with a volume ratio of clinopyroxene to spinel of approximately 50:1. Similar Al-rich compositions have been observed in chromian spinel grains from the Rum layered intrusion, Scotland (Henderson 1975, Henderson & Wood 1981); the Al-enrichment trend was proposed to result from a reaction relationship involving chromite, olivine and either plagioclase or interstitial melt rich in the plagioclase component. The absence of plagioclase in ultramafic rocks from the Turnagain intrusion and the physical setting of the Al-rich chromian spinel grains within large oikocrysts of clinopyroxene suggest that the re-equilibration of spinel with clinopyroxene is an additional mechanism for producing the Al-enrichment trend spinel compositional trend in mafic–ultramafic rocks.

Finally, the chromian spinel compositions from two samples of dunite (04ES–03–02–01 and 04ES–08–01–01) extend nearly parallel to the Cr–Fe^{3+} join, with $Fe^{3+}/(Fe^{3+} + Cr + Al) > 0.18$ (trend 4 in Fig. 8A) and increasing $Fe^{2+}/(Fe^{2+} + Mg)$ (Fig. 6), and they appear to have been modified both by oxygenated fluids and subsolidus re-equilibration with olivine. The majority of the spinel grains in these two samples of dunite occur along olivine grain-boundaries, not inside olivine. The increase in $Fe^{3+}/(Fe^{3+} + Cr + Al)$ may be attributed to oxidation by fluids that locally precipitated magnetite. The grains of chromian spinel from these two dunite samples show little to no enrichment in Al or Ti (Figs. 6B, 7A [group 4]), which suggests that they did not re-equilibrate with evolved, interstitial melt. The increasing $Fe^{2+}/(Fe^{2+} + Mg)$ in these spinel grains thus appears to be the result of Fe^{2+}–Mg subsolidus exchange between olivine and spinel during cooling (Clark 1978), perhaps aided by circulating fluids.

Compositional effects of serpentinization

Magnetite and Fe^{3+}-rich chromite forming a rim around chromian spinel grains in many rocks from the Turnagain intrusion are a result of serpentinization. Where sufficiently wide to analyze with an electron beam 10 μm wide, such rims exhibit compositions distinct from primary spinel compositions in the chromitites and high-temperature re-equilibrated compositions documented above. Compositions from the dunite, wehrlite, and olivine clinopyroxenite samples that plot near the Fe^{3+} apex in Figure 5A are Cr-bearing magnetite (with little to no detectable Al) and likely reflect nucleation of magnetite around pre-existing chromite during serpentinization. Compared to chromian spinel, rims of Fe^{3+}-rich chromite are characterized by lower Cr, slightly lower Al, and higher Fe^{3+} (Fig. 5A) and higher $Fe^{3+}/(Fe^{2+} + Fe^{3+})$ (Fig. 5B), and appear to reflect the Fe-rich and Cr-poor nature of the fluids from which these rims formed. Some samples contain individual grains with an inner Fe^{3+}-rich chromite rim and an outer magnetite rim (*e.g.,* 04ES–03–02–01). This observation suggests that Fe^{3+}-rich chromite represents a reaction product between fluids and chromite with a core-to-rim order of formation of chromite → Fe^{3+}-rich chromite → magnetite.

Comparison with chromian spinel compositions from other Alaskan-type intrusions

The compositions of chromian spinel from the Turnagain intrusion are distinctive from those determined for Alaskan-type intrusions worldwide. In an expanded view of the Fe^{3+}–Cr–Al triangular plot (Fig. 8B), all compositions of spinel cores from this study are plotted by lithology together with the 90% data density contours for spinel compositions for other Alaskan-type intrusions (number of datasets = 386) as compiled by Barnes & Roeder (2001). The majority of the chromian spinel compositions from the Turnagain intrusion lie to lower $Fe^{3+}/(Fe^{3+} + Cr + Al)$ than the established compositional field, and they are also have lower $Fe^{3+}/(Fe^{3+} + Cr + Al)$ than the recently published chromian spinel dataset (number of datasets = 1326) of Krause *et al.* (2007) from Uralian–Alaskan-type complexes in the Ural Mountains (Kytlym, Svetley Bor, Nizhnii Tagil). With respect to the Fe^{3+}–Cr–Al plot, chromian spinel from the Turnagain intrusion is similar in composition to spinel from boninites and island-arc tholeiites in the compilation of Barnes & Roeder (2001) (Fig. 8B).

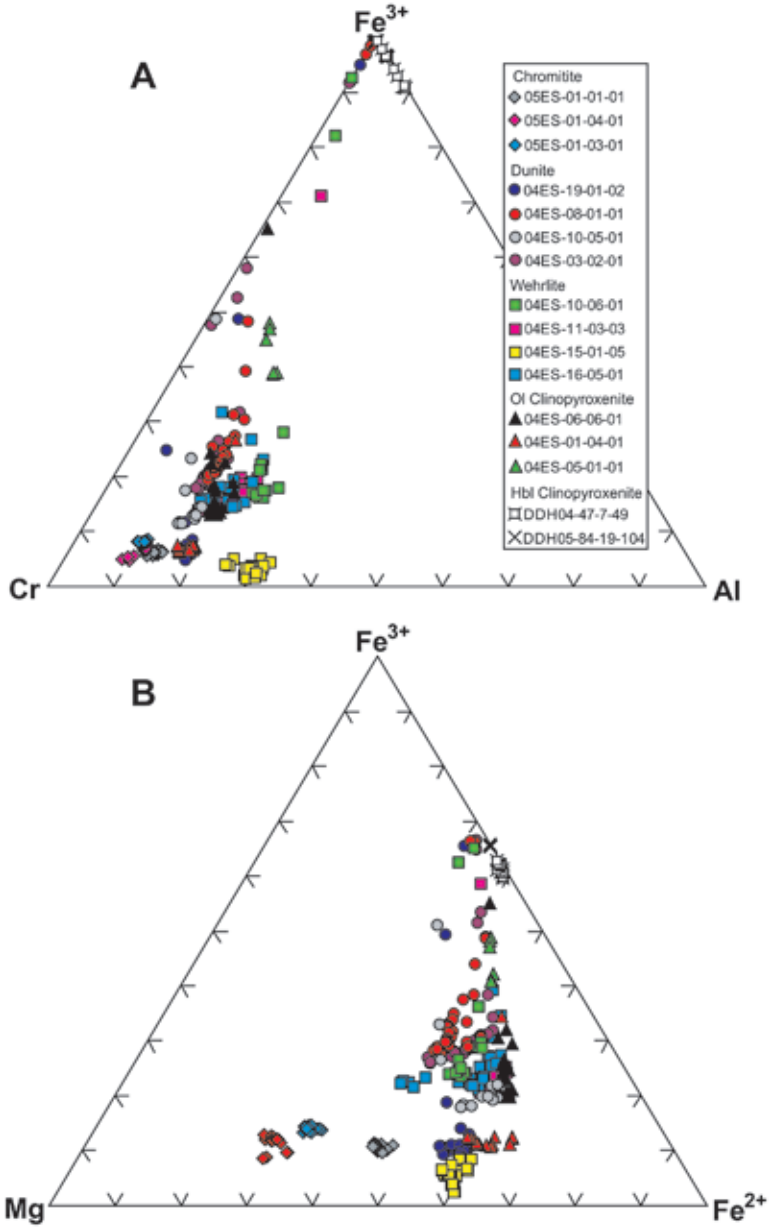

FIG. 5. Triangular diagrams showing spinel compositions. A) Plot of trivalent cations (Fe^{3+}–Cr–Al) showing all spinel compositions from Turnagain represented by sample number. B) Triangular Mg–Fe^{2+}–Fe^{3+} plot of all spinel compositions from Turnagain. Symbols: ol: olivine, hbl: hornblende.

Implications for the redox state of the Turnagain intrusion and presence of magmatic sulfide mineralization

Most Alaskan-type intrusions appear to have formed from relatively oxidized arc-type magmas, with estimated ΔlogFMQ (log units of oxygen fugacity relative to the fayalite – magnetite – quartz synthetic buffer) values between +1 to +3.5 (*e.g.,* Ballhaus *et al*. 1991, Carmichael 1991, Garuti *et al*. 2003, Rohrbach *et al*. 2005). Under such oxidized conditions, sulfur should exist mainly as sulfate (SO_4^{2-}) rather than sulfide (S^{2-}) species in the melt (Jugo *et al*. 2004, 2005). The presence of significant amounts of magmatic sulfide associated with dunite and wehrlite in the southeastern parts of the Turnagain intrusion indicates that some of the magmas indeed achieved local saturation in sulfide. The relative oxygen fugacity for the magmas that crystallized to form these rocks must therefore have been low enough for the predominance of dissolved sulfide over sulfate (less than ΔlogFMQ ~1; Jugo *et al*. 2005) and more reduced than that for typical Alaskan-type intrusions.

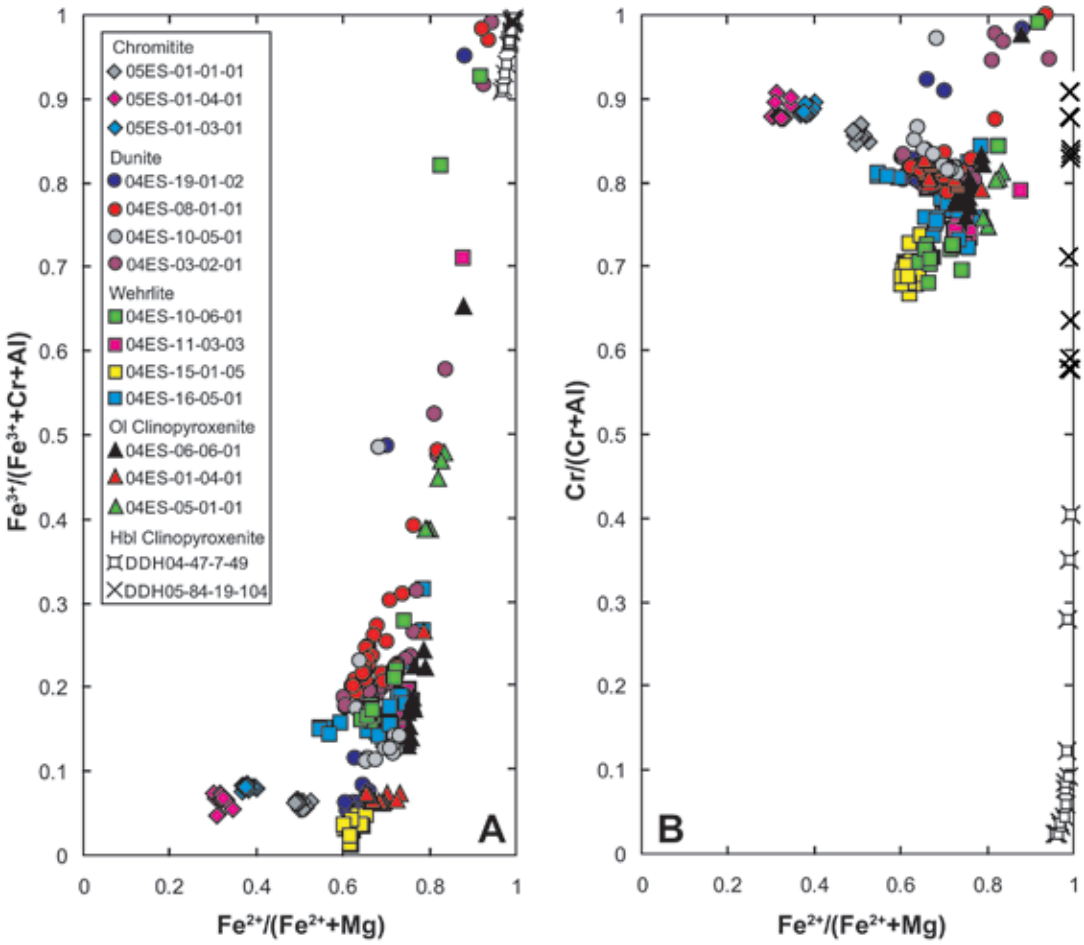

FIG. 6. Binary diagrams showing $Fe^{2+}/(Fe^{2+} + Mg)$ variations in spinel compositions from the Turnagain intrusion, represented by sample number. These plots are projections of the spinel prism (Irvine 1965). A) $Fe^{2+}/(Fe^{2+} + Mg)$ *versus* $Fe^{3+}/(Fe^{3+} + Cr + Al)$, or divalent *versus* trivalent cation plot. A distinct Fe-enrichment trend exists for most chromian spinel compositions from the Turnagain intrusion, a typical feature of Alaskan-type intrusions, with the exception of magnesiochromite grains from the chromitites and other grains with $Fe^{3+}/(Fe^{3+} + Cr + Al)$ less than 0.1. B) $Fe^{2+}/(Fe^{2+} + Mg)$ *versus* $Cr/(Cr + Al)$. Magnesiochromite grains from the chromitites have significantly lower $Fe^{2+}/(Fe^{2+} + Mg)$ and higher $Cr/(Cr + Al)$ compared to other chromian spinel compositions.

TABLE 1. REPRESENTATIVE COMPOSITIONS OF SPINEL FROM SPINEL-BEARING ULTRAMAFIC ROCKS OF THE TURNAGAIN ALASKAN-TYPE INTRUSION, BRITISH COLUMBIA, CANADA

Rock	Chromitite			Dunite			Dunite			Dunite			Wehrlite		
Sample	05ES			04ES			04ES			04ES			04ES		
	01-04-01			19-01-02			03-02-01			08-01-01			11-03-03		
Cluster	6-1			2-1			5-1			2-1			4-2		
Texture	l. anh.			s. anh.			l. sub.			s. euh.			m. sub.		
Zone	Core	Mid	Rim	Core	Mid	Rim	Core	Mid	Rim	Core	Mid	Rim	Core	Mid	Rim
SiO_2 wt.%	0.00	0.00	0.00	0.02	0.06	0.03	0.02	0.03	0.08	0.03	0.03	0.05	0.00	0.00	0.01
TiO_2	0.22	0.27	0.22	0.79	0.94	0.76	0.47	0.45	0.02	0.52	0.54	0.53	1.35	1.28	1.26
Al_2O_3	5.94	5.80	5.07	8.98	8.99	8.73	6.72	6.85	0.02	7.35	7.28	7.47	10.23	10.27	10.47
Cr_2O_3	62.86	62.85	65.24	54.58	54.66	54.61	50.24	44.90	0.57	46.49	46.40	44.81	44.37	43.96	43.31
V_2O_3	0.05	0.02	0.02	0.10	0.14	0.18	0.07	0.10	0.02	0.07	0.09	0.06	0.32	0.29	0.30
Fe_2O_3	5.82	5.43	3.82	4.71	4.31	5.15	13.72	17.07	68.76	15.97	15.98	16.75	11.65	12.24	13.03
FeO	11.78	11.59	11.22	22.75	22.84	23.24	21.46	24.94	29.45	22.94	22.81	22.94	26.10	26.04	26.18
MnO	0.00	0.02	0.04	0.34	0.32	0.42	0.25	0.38	0.14	0.22	0.22	0.24	0.31	0.34	0.40
MgO	14.14	14.09	14.19	7.12	7.17	6.86	7.79	5.23	0.93	6.84	6.90	6.64	5.54	5.52	5.50
NiO	0.17	0.16	0.13	n.d.	n.d.	n.d.	n.d.	n.d.	n.d.	n.d.	n.d.	n.d.	n.d.	n.d.	n.d.
CaO	0.01	0.01	0.00	0.01	0.03	0.00	0.01	0.02	0.01	0.02	0.01	0.00	0.01	0.00	0.01
Total	100.99	100.26	99.96	99.42	99.46	99.99	100.74	99.95	99.99	100.46	100.26	99.48	99.87	99.95	100.45
Ti *apfu*	0.005	0.007	0.006	0.020	0.024	0.019	0.012	0.012	0.000	0.013	0.014	0.014	0.035	0.033	0.032
Cr	1.615	1.626	1.695	1.472	1.472	1.469	1.351	1.240	0.017	1.260	1.259	1.227	1.202	1.190	1.167
Al	0.228	0.224	0.196	0.361	0.361	0.350	0.270	0.282	0.001	0.297	0.295	0.305	0.413	0.414	0.420
V	0.001	0.001	0.000	0.002	0.003	0.004	0.002	0.002	0.000	0.002	0.002	0.001	0.007	0.007	0.007
Fe^{3+}*	0.142	0.134	0.094	0.121	0.110	0.132	0.351	0.449	1.977	0.412	0.413	0.436	0.300	0.315	0.334
Fe^{2+}*	0.320	0.317	0.308	0.649	0.651	0.661	0.610	0.729	0.941	0.657	0.655	0.664	0.748	0.746	0.746
Mn	0.000	0.001	0.001	0.010	0.009	0.012	0.007	0.011	0.005	0.006	0.006	0.007	0.009	0.010	0.012
Mg	0.685	0.688	0.695	0.362	0.364	0.348	0.395	0.272	0.053	0.349	0.353	0.343	0.283	0.282	0.279
Ni	0.004	0.004	0.004	n.d.	n.d.	n.d.	n.d.	n.d.	n.d.	n.d.	n.d.	n.d.	n.d.	n.d.	n.d.
Ca	0.000	0.000	0.000	0.000	0.001	0.000	0.000	0.001	0.000	0.001	0.000	0.000	0.000	0.000	0.000
Total	3.001	3.001	3.001	2.998	2.995	2.997	2.998	2.997	2.995	2.998	2.998	2.997	2.997	2.997	2.997
End members based on the dominant trivalent cation															
Cr/Σ3+	0.814	0.820	0.854	0.753	0.757	0.753	0.685	0.629	0.009	0.640	0.640	0.623	0.628	0.620	0.607
Al/Σ3+	0.115	0.113	0.099	0.185	0.186	0.179	0.137	0.143	0.000	0.151	0.150	0.155	0.216	0.216	0.219
Fe/Σ3+	0.072	0.067	0.048	0.062	0.057	0.068	0.178	0.228	0.991	0.209	0.210	0.222	0.157	0.164	0.174

Cluster: the first number indicates the cluster of grains, and the second number indicates the specific grain analyzed within the cluster. Texture: euh. (euhedral), sub. (subhedral), anh. (anhedral), interg. (intergrown), irreg. (irregular); l. (large), m. (medium), s. (small). n.d.: not determined. * The amounts of Fe^{2+} and Fe^{3+} are determined by stoichiometry.

The oxygen fugacity of the parent magmas to the Turnagain intrusion would have largely been controlled by the redox conditions of the mantle source during partial melting, decompression during ascent through the lithosphere, and mineral–melt equilibria during crystallization (*e.g.,* Carmichael 1991, Lindsley & Frost 1992, Ballhaus & Frost 1994). Although the composition of chromian spinel alone is not sufficient to quantitatively constrain oxygen fugacity, the combination of low $Fe^{3+}/(Fe^{3+} + Cr + Al)$, low $Fe^{3+}/(Fe^{2+} + Fe^{3+})$, and high $Cr/(Cr + Al)$ values of magnesiochromite grains from the chromitites and of the least re-equilibrated chromite grains from the dunites and wehrlites are consistent with relatively low $Fe^{3+} : Fe^{2+}$ values in the parental magmas of the Turnagain intrusion (*e.g.,* Parkinson & Arculus 1999). Reduction and sulfide saturation of the Turnagain parental magmas may have been achieved by the local assimilation of graphitic and pyritic phyllite wallrocks (Nixon 1998), which are found as inclusions in drillcore only in the sulfide-mineralized zones hosted by dunite–wehrlite. This process is supported by sulfur isotopic values from sulfide mineral separates in the intrusion, in the range from $\delta^{34}S$ range from –9.7 to +1.4‰; the lightest values correspond to samples of mineralized dunite and wehrlite, and trend toward the composition of sulfide from the phyllite (–17.9‰: Scheel 2007). Assimilation of the pyrite-bearing phyllite would also have added sulfur to the magma, thus aiding saturation in a sulfide liquid.

TABLE 1 (cont'd). REPRESENTATIVE COMPOSITIONS OF SPINEL FROM SPINEL-BEARING ULTRAMAFIC ROCKS OF THE TURNAGAIN ALASKAN-TYPE INTRUSION, BRITISH COLUMBIA, CANADA

Rock	Wehrlite			Wehrlite			Olivine Clinopyroxenite			Olivine Clinopyroxenite			Hbl Clinopyroxenite		
Sample	04ES			04ES			04ES			05ES			DDH04		
	16-08-01			10-06-01			06-06-01			05-01-01			47-7-49		
Cluster	6-3			1-2			4.5-2			8-1			5-1		
Texture	s. euh.			m. anh.			m. anh.			s. euh.			l. anh.		
Zone	Core	Mid	Rim	Core	Mid	Rim	Core	Mid	Rim	Core	Mid	Rim	Core	Mid	Rim
SiO_2 wt.%	0.03	0.03	0.01	0.00	0.03	0.03	0.02	0.00	0.01	0.03	0.00	0.03	0.03	0.03	0.03
TiO_2	1.03	1.05	1.03	0.89	0.94	0.11	1.02	0.98	0.84	2.51	2.48	2.42	3.27	3.19	0.35
Al_2O_3	7.99	7.85	7.99	11.86	12.00	0.03	8.35	8.61	8.25	4.64	4.44	4.18	2.27	1.12	0.16
Cr_2O_3	50.02	50.34	49.53	42.92	42.33	4.83	48.48	48.60	46.95	28.34	27.45	26.90	0.13	0.15	0.13
V_2O_3	0.09	0.08	0.08	0.16	0.20	0.00	0.22	0.24	0.25	0.11	0.08	0.07	0.46	0.45	0.73
Fe_2O_3	10.92	11.46	11.56	13.33	13.34	64.67	10.11	9.68	11.33	30.20	31.67	32.01	59.94	60.85	67.39
FeO	20.46	19.79	20.19	24.21	24.16	28.70	26.30	26.26	25.75	25.09	25.31	25.19	34.04	33.83	31.82
MnO	0.20	0.25	0.18	0.30	0.37	0.35	0.41	0.35	0.78	4.07	3.92	3.87	0.26	0.22	0.02
MgO	8.70	9.22	8.88	6.70	6.68	1.43	4.92	4.96	4.70	3.08	2.98	2.79	0.46	0.29	0.15
NiO	n.d.	n.d.	n.d.	n.d.	n.d.	n.d.	n.d.	n.d.	n.d.	n.d.	n.d.	n.d.	n.d.	n.d.	n.d.
CaO	0.00	0.01	0.00	0.01	0.00	0.00	0.01	0.01	0.03	0.17	0.26	0.34	0.03	0.00	0.01
Total	99.43	100.09	99.45	100.39	100.05	100.17	99.85	99.69	98.90	98.24	98.60	97.80	100.90	100.12	100.78
Ti *apfu*	0.026	0.027	0.026	0.023	0.024	0.003	0.027	0.026	0.022	0.069	0.068	0.067	0.092	0.091	0.010
Cr	1.343	1.340	1.329	1.140	1.127	0.145	1.330	1.333	1.303	0.821	0.795	0.787	0.004	0.004	0.004
Al	0.320	0.311	0.320	0.470	0.476	0.002	0.342	0.352	0.341	0.200	0.192	0.182	0.100	0.050	0.007
V	0.002	0.002	0.002	0.004	0.005	0.000	0.005	0.005	0.006	0.003	0.002	0.002	0.011	0.011	0.018
Fe3+*	0.279	0.290	0.295	0.337	0.338	1.846	0.264	0.253	0.299	0.833	0.873	0.891	1.687	1.739	1.929
Fe2+*	0.581	0.557	0.573	0.680	0.681	0.910	0.763	0.762	0.756	0.769	0.775	0.779	1.064	1.074	1.012
Mn	0.006	0.007	0.005	0.009	0.011	0.011	0.012	0.010	0.023	0.126	0.122	0.121	0.008	0.007	0.001
Mg	0.440	0.463	0.449	0.336	0.335	0.081	0.255	0.257	0.246	0.168	0.163	0.154	0.026	0.017	0.008
Ni	n.d.	n.d.	n.d.	n.d.	n.d.	n.d.	n.d.	n.d.	n.d.	n.d.	n.d.	n.d.	n.d.	n.d.	n.d.
Ca	0.000	0.000	0.000	0.000	0.000	0.000	0.000	0.000	0.001	0.007	0.010	0.014	0.001	0.000	0.001
Total	2.998	2.998	2.999	2.998	2.997	2.998	2.997	2.998	2.997	2.997	2.999	2.998	2.993	2.994	2.990
End members based on the dominant trivalent cation															
Cr/Σ3+	0.692	0.690	0.684	0.586	0.581	0.073	0.687	0.688	0.670	0.443	0.428	0.423	0.002	0.002	0.002
Al/Σ3+	0.165	0.160	0.164	0.241	0.245	0.001	0.176	0.182	0.176	0.108	0.103	0.098	0.056	0.028	0.004
Fe/Σ3+	0.144	0.150	0.152	0.173	0.174	0.926	0.136	0.130	0.154	0.449	0.469	0.479	0.942	0.970	0.994

Cluster: the first number indicates the cluster of grains, and the second number indicates the specific grain analyzed within the cluster. Texture: euh. (euhedral), sub. (subhedral), anh. (anhedral), interg. (intergrown), irreg. (irregular); l. (large), m. (medium), s. (small). n.d.: not determined. * The amounts of Fe^{2+} and Fe^{3+} are determined by stoichiometry.

CONCLUSIONS

The principal results of this study can be summarized as follows:

(1) primary or near-primary spinel compositions in the Turnagain intrusion of northern British Columbia, Canada, are relatively Fe^{3+}-poor and Cr-rich compared to published results from Alaskan-type intrusions worldwide, especially magnesiochromite grains from chromitite layers and pods in the intrusion;

(2) grains of chromian spinel from dunite, wehrlite and olivine clinopyroxenite exhibit systematic within-sample trends that can be related to a variety of processes, including olivine fractionation, re-equilibration with interstitial melt, re-equilibration with coexisting silicate phases, oxidation, and serpentinization;

(3) the low $Fe^{3+}/(Fe^{3+} + Cr + Al)$, low $Fe^{3+}/(Fe^{2+} + Fe^{3+})$, and high $Cr/(Cr + Al)$ values from the magnesiochromite grains from the chromitites are consistent with crystallization from magmas characterized by a relatively low oxygen fugacity compared to other Alaskan-type intrusions (less than $\Delta\log FMQ \approx 1$). The reduced nature of the parental magmas and addition of external sulfur, attributed to the assimilation of graphitic and pyritic country-rocks, likely promoted local saturation in a sulfide liquid.

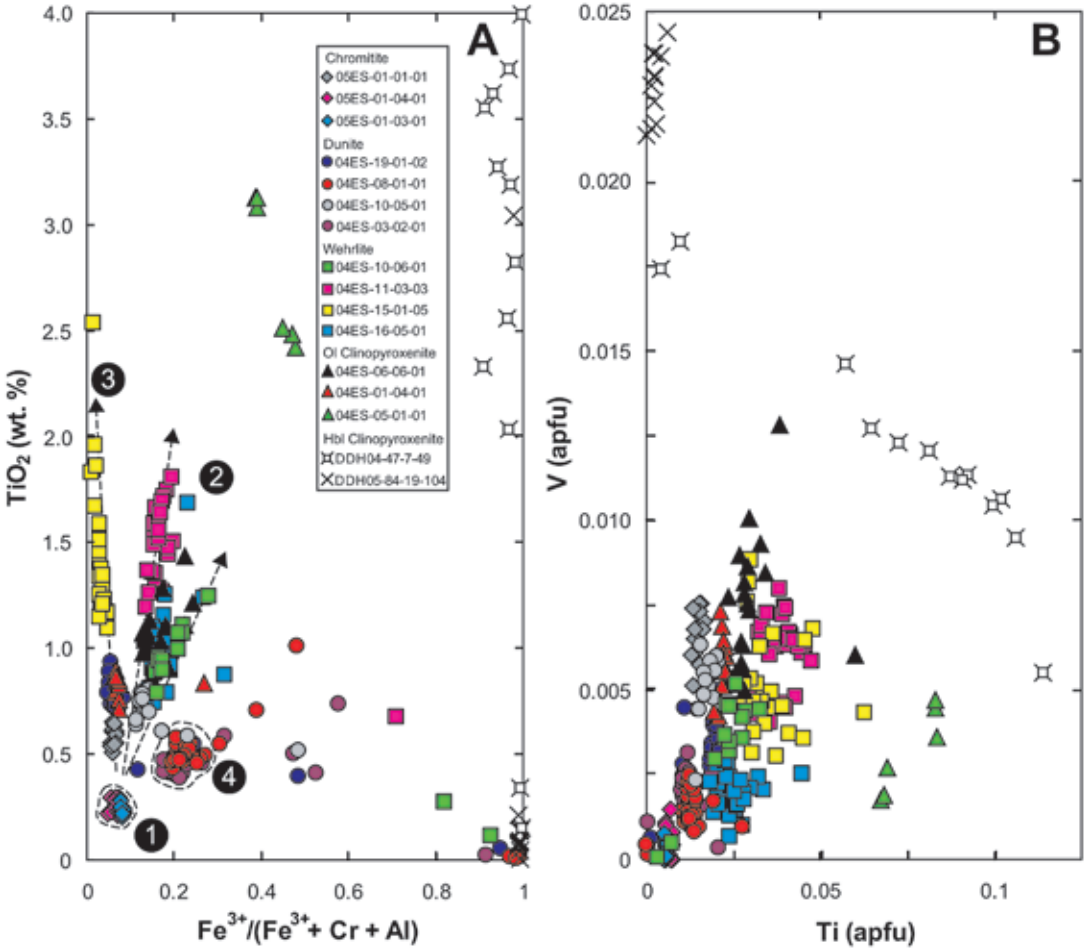

FIG. 7. Binary diagrams showing titanium variations in spinel compositions from the Turnagain intrusion. Abbreviations as indicated in Figure 5. A) $Fe^{3+}/(Fe^{3+} + Cr + Al)$ *versus* TiO_2. Spinel compositions from the Turnagain intrusion show a wide range of Ti contents; four distinct groups or trends are identified on the diagram (excluding Fe^{3+}-rich chromite and magnetite). Group 1 consists of grains from the two samples of chromitite (05ES–01–04–01 and 05ES–01–03–01) that have the lowest TiO_2 and $Fe^{3+}/(Fe^{3+} + Cr + Al)$ value of all chromian spinel compositions and reflect the least amount of re-equilibration. Arrows indicate vectors of increasing $Fe^{3+}/(Fe^{3+} + Cr + Al)$ and TiO_2 for re-equilibration with evolved interstitial liquid (trend 2) and increasing TiO_2 with decreasing $Fe^{3+}/(Fe^{3+} + Cr + Al)$ for re-equilibration with clinopyroxene (trend 3). Also identified are chromian spinel compositions (group 4) from two dunite samples (04ES–08–01–01 and 04ES–03–02–01) that cluster together at low TiO_2 contents (~0.5 wt.%). See Discussion for additional details. B) Ti *versus* V (*apfu*). Most samples are characterized by nearly vertical trends with the exception of magnetite from DDH04–47–7–49. Note the vanadium enrichment of magnetite from sample DDH05–84–19–104.

FIG. 8. Expanded view of the Cr apex region of the Fe^{3+}–Cr–Al diagram showing only core compositions of spinel from the Turnagain intrusion (*i.e.*, no rim compositions are plotted). The inset in center-left part of the diagram shows the entire diagram and the region represented by the expanded view (grey field). A) Compositions of chromian spinel represented by sample number. The four groups or trends identified in Figure 7A are also noted. Magnesiochromite grains from the two chromitites (05ES–01–04–01 and 05ES–01–03–01) have the lowest $Fe^{3+}/(Fe^{3+} + Cr + Al)$, $Fe^{2+}/(Fe^{2+} + Mg)$ and TiO_2 values, and the highest Cr/Al value of all spinel grains analyzed in this study, and plot closest to the Cr apex of the diagram (group 1). Arrows indicate vectors for re-equilibration with evolved interstitial liquid (trend 2), re-equilibration with clinopyroxene (trend 3), and combined re-equilibration with olivine and oxidation (trend 4) in dunite samples 04ES–08–01–01 and 04ES–03–02–01. All trends converge towards the area of the encircled compositions from the chromitites. B) Compositions of chromian spinel rep-

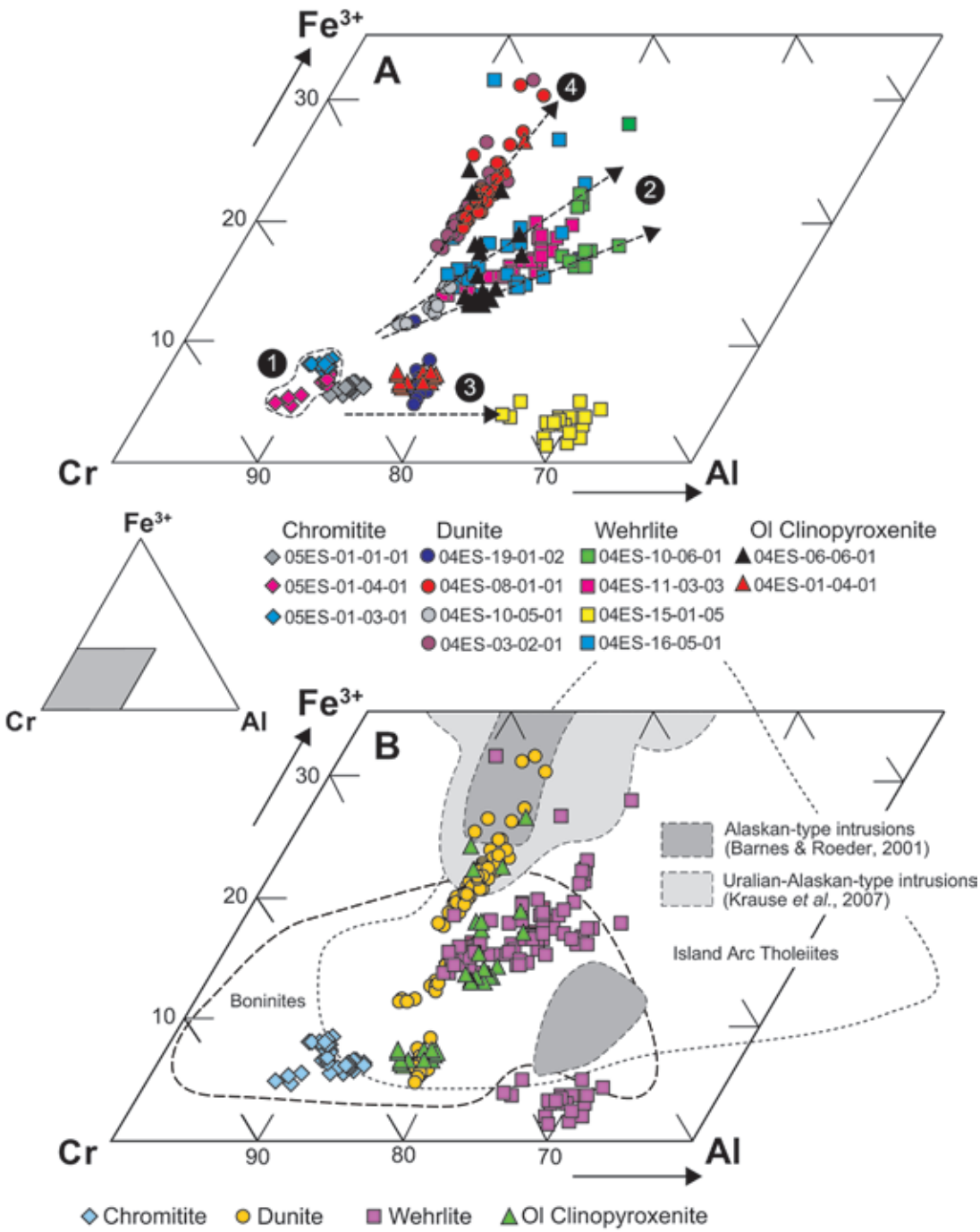

resented by rock type. Grey-filled fields show the distribution of spinel compositions from Alaskan-type intrusions worldwide, including the 90% density maxima for spinel compositions (n = 386) from Barnes & Roeder (2001) [the 50% maximum plots off the diagram to higher $Fe^{3+}/(Fe^{3+} + Cr + Al)$] and spinel compositions (n = 1326) from Uralian–Alaskan-type intrusions in the Ural Mountains from Krause *et al*. (2007; Fig. 4F). Also added for reference are the 90% density maxima for boninites (long-dashed line) and island-arc tholeiites (short-dashed line) from the Barnes & Roeder (2001) compilation.

Acknowledgements

We thank Mati Raudsepp at the University of British Columbia for training and guidance in the use the electron microprobe throughout this study. Stephen J. Barnes provided us with the Barnes & Roeder (2001) spinel database and spreadsheet for data reduction. Caroline-Emmanuelle Morisset, Jon Scoates, Greg Dipple, and Jim Mortensen provided valuable input on earlier versions of this manuscript. Careful reviews by Marco Fiorentini and Evgeny Pushkarev, and editorial assistance from Robert Martin, were especially useful. The authors are grateful to Hard Creek Nickel Corp. for field support for this project and to Jim Reed of Pacific Western Helicopters for his exemplary logistical support in the field. Special thanks to Tony Hitchins, Bruce Northcote, Chris Baldys, and Mark Jarvis (President) of Hard Creek Nickel Corp. for their generous support and interactions throughout the period of the principal author's M.Sc. thesis at UBC. Funding for this project was provided by a research grant from Hard Creek Nickel Corp. (formerly Canadian Metals Exploration Ltd.) and a NSERC Discovery Grant to J.S. Scoates.

References

Ballhaus, C., Berry, R.F. & Green, D.H. (1991): High pressure experimental calibration of the olivine – orthopyroxene – spinel oxygen geobarometer: implications for the oxidation state of the upper mantle. *Contrib. Mineral. Petrol.* **107**, 27-40.

Ballhaus, C. & Frost, B.R. (1994): The generation of oxidized CO_2-bearing basaltic melts from reduced CH_4-bearing upper mantle sources. *Geochim. Cosmochim. Acta* **58**, 4931-4940.

Barnes, S.J. (1998): Chromite in komatiites. 1. Magmatic controls on crystallization and composition. *J. Petrol.* **39**, 1689-1720.

Barnes, S.J. & Brand, N.W. (1999): The distribution of Cr, Ni and chromite in komatiites, and application to exploration for komatiite-hosted nickel sulfide deposits. *Econ. Geol.* **94**, 129-132.

Barnes, S.J. & Roeder, P.L. (2001): The range of spinel compositions in terrestrial mafic and ultramafic rocks. *J. Petrol.* **42**, 2279-2302.

Carmichael, I.S.E. (1991): The redox states of basic and silicic magmas: a reflection of their source regions? *Contrib. Mineral. Petrol.* **106**, 129-141.

Clark, T. (1975): *Geology of an Ultramafic Complex on the Turnagain River, Northwestern B.C.* Ph.D. thesis, Queen's University, Kingson, Ontario.

Clark, T. (1978): Oxide minerals in the Turnagain ultramafic complex, northwestern British Columbia. *Can. J. Earth Sci.* **15**, 1893-1903.

Clark, T. (1980): Petrology of the Turnagain ultramafic complex, northwestern British Columbia. *Can. J. Earth Sci.* **17**, 744-757.

Dick, H.J.B. & Bullen, T. (1984): Chromian spinel as a petrogenetic indicator in abyssal and alpine-type peridotites and spatially associated lavas. *Contrib. Mineral. Petrol.* **86**, 54-76.

Erdmer, P., Mihalynuk, M.G., Gabrielse, H., Heaman, L.M. & Creaser, R.A. (2005): Mississippian volcanic assemblage conformably overlying Cordilleran miogeoclinal strata, Turnagain River area, northern British Columbia, is not part of an accreted terrane. *Can. J. Earth Sci.* **42**, 1449-1465.

Findlay, D.C. (1969): Origin of the Tulameen ultramafic – gabbro complex, southern British Columbia. *Can. J. Earth Sci.* **6**, 399-425.

Fiorentini, M.L., Beresford, S.W. & Barley, M.E. (2008): Ruthenium–chromium variation: a new lithogeochemical tool in the exploration for komatiite-hosted Ni–Cu–(PGE) deposits. *Econ. Geol.* **103**, 431-437.

Foster, F. (1974): *History and Origin of the Polaris Ultramafic Complex in the Aiken Lake Area of North-Central British Columbia*. B.Sc. thesis, Univ. British Columbia, Vancouver, British Columbia.

Gabrielse, H. (1998): Geology of Cry Lake and Dease Lake map areas, north-central British Columbia. *Geol. Surv. Can., Bull.* **504**.

Garuti, G., Pushkarev, E.V., Zaccarini, F., Cabella, R. & Anikina, E. (2003): Chromite composition and platinum-group mineral assemblage in the Uktus Uralian–Alaskan-type complex (Central Urals, Russia). *Mineral. Deposita* **38**, 312-326.

Henderson, P. (1975): Reaction trends shown by chrome-spinels of the Rhum layered intrusion. *Geochim. Cosmochim. Acta* **39**, 1035-1044.

Henderson, P. & Wood, R.J. (1981): Reaction relationships of chrome-spinels in igneous rocks – further evidence from the layered intrusions of Rhum and Mull, Inner Hebrides, Scotland. *Contrib. Mineral. Petrol.* **78**, 225-229.

Irvine, T.N. (1965): Chromian spinel as a petrogenetic indicator. I. Theory. *Can. J. Earth Sci.* **2**, 648-672.

Irvine, T.N. (1967): Chromian spinel as a petrogenetic indicator. II. Petrologic applications. *Can. J. Earth Sci.* **4**, 71-103.

Irvine, T.N. (1974): Petrology of the Duke Island ultramafic complex, southeastern Alaska. *Geol. Soc. Am., Mem.* **138**.

Irvine, T.N. (1987): Layering and related structures in the Duke Island and Skaergaard intrusions: similarities, differences, and origins. *In* Origins of Igneous Layering (I. Parsons, ed.). D. Reidel Publishing, Dordrecht, The Netherlands (185-245).

JUGO, P.J., LUTH, R.W. & RICHARDS, J.P. (2004): Experimental data on the speciation of sulfur as a function of oxygen fugacity in basaltic melts. *Geochim. Cosmochim. Acta* **69**, 497-503.

JUGO, P.J., LUTH, R.W. & RICHARDS, J.P. (2005): An experimental study of the sulfur content in basaltic melts saturated with immiscible sulfide or sulfate liquids at 1300°C and 1.0 GPa. *J. Petrol.* **46**, 783-798.

KAMENETSKY, V.S., CRAWFORD, A.J. & MEFFRE, S. (2001): Factors controlling chemistry of magmatic spinel: an empirical study of associated olivine, chrome-spinel and melt inclusion from primitive rocks. *J. Petrol.* **42**, 655-671.

KAMPERMAN, M., DANYUSHEVSKY, L.V., TAYLOR, W.R. & JABLONSKI, W. (1996): Direct oxygen measurements of Cr-rich spinel: implications for spinel stoichiometry. *Am. Mineral.* **81**, 1186-1194.

KRAUSE, J., BRÜGMANN, G.E. & PUSHKAREV, E.V. (2007): Accessory and rock forming minerals monitoring the evolution of zoned mafic–ultramafic complexes in the central Ural Mountains. *Lithos* **95**, 19-42.

LINDSLEY, D.H. & FROST, B.R. (1992): Equilibria among Fe–Ti oxides, pyroxenes, olivine, and quartz. I. Theory. *Am. Mineral.* **77**, 987-1003.

MELLINI, M., RUMORI, C. & VITI, C. (2005): Hydrothermally reset magmatic spinels in retrograde serpentinites: formation of "ferritchromit" rims and chlorite aureoles. *Contrib. Mineral. Petrol.* **149**, 266-275.

NIXON, G.T. (1998): Ni-sulphide mineralization in the Turnagain Alaskan-type complex: a unique magmatic environment. *B.C. Ministry of Energy, Mines and Petroleum Resources, Pap.* **1998-1**, 18-1 – 18-12.

NIXON, G.T., HAMMACK, J.L., ASH, C.H., CABRI, L.J., CASE, G., CONNELLY, J.N., HEAMAN, L.M., LAFLAMME, J.H.G., NUTTALL, C., PATERSON, W.P.E. & WONG, R.H. (1997): Geology and platinum-group-element mineralization of Alaskan-type ultramafic–mafic complexes in British Columbia. *B.C. Ministry of Employment and Investment, Bull.* **93**.

PARKINSON, I.J. & ARCULUS, R.J. (1999): The redox state of subduction zones: insights from arc-peridotites. *Chem. Geol.* **160**, 409-423.

POUCHOU, J.L. & PICHOIR, F. (1985): PAP $\phi(\rho Z)$ procedure for improved quantitative microanalysis. *Microbeam Anal.*, 104-106.

POUSTOVETOV, A.A. & ROEDER, P.L. (2001): The distribution of chromium between basaltic melt and chromian spinel as an oxygen geobarometer. *Can. Mineral.* **39**, 309-317.

POWER, M.R., PIRRIE, D., ANDERSON, J.C.Ø. & WHEELER, P.D. (2000): Testing the validity of chrome spinel chemistry as a provenance and petrogenetic indicator. *Geology* **28**, 1027-1030.

ROEDER, P.L. (1994): Chromite: from the fiery rain of chondrules to the Kilauea Iki lava lake. *Can. Mineral.* **32**, 729-746.

ROEDER, P.L. & CAMPBELL, I.H. (1985): The effect of postcumulus reactions on composition of chrome-spinels from the Jimberlana intrusion. *J. Petrol.* **26**, 763-786.

ROEDER, P.L., POUSTOVETOV, A.A. & OSKARSSON, N. (2001): Growth forms and composition of chromian spinel in MORB magma: diffusion-controlled crystallization of chromian spinel. *Can. Mineral.* **39**, 397-416.

ROEDER, P.L. & REYNOLDS, I. (1991): Crystallization of chromite and chromium stability in basaltic melts. *J. Petrol.* **32**, 909-934.

ROHRBACH, A., SCHUTH, S., BALLHAUS, C., MÜNKER, C., MATVEEV, S. & QOPOTO, C. (2005): Petrological constraints on the origin of arc picrites, New Georgia Group, Solomon Islands. *Contrib. Mineral. Petrol.* **149**, 685-698.

SACK, R.O. & GHIORSO, M.S. (1991): Chromite as a petrogenetic indicator. *In* Oxide Minerals (D.H. Lindsley, ed.). *Rev. Mineral.* **25**, 323-354.

SCHEEL, J.E. (2007): *Age and Origin of the Turnagain Alaskan-type Intrusion and Associated Ni-Sulphide Mineralization, North-Central British Columbia, Canada*. M.Sc. thesis, Univ. British Columbia, Vancouver, British Columbia.

SCOWEN, P.A.H., ROEDER, P.L. & HELZ, R.T. (1991): Reequilibration of chromite within Kilauea Iki lava lake, Hawaii. *Contrib. Mineral. Petrol.* **107**, 8-20.

SIMPSON, P.A.H. (2007): Mineral resource update, Turnagain Nickel Project. *GeoSim Services Inc., Tech. Rep.* (*unpubl.*).

TAYLOR, H.P., JR. (1967): The zoned ultramafic complexes of southern Alaska. *In* Ultramafic and Related Rocks (P.J. Wyllie, ed.). Wiley, New York, N.Y. (97-121).

Received March 3, 2008, revised manuscript accepted January 17, 2009.

APPENDIX 1. SAMPLE LOCATIONS, TURNAGAIN ALASKAN-TYPE COMPLEX, NORTHERN BRITISH COLUMBIA

Number	Sample #	Rock Type	Easting	Northing
1	05ES-01-01-01	Chromitite	506969	6483816
2	05ES-01-04-01	Chromitite	507440	6484076
3	05ES-01-03-01	Chromitite	507319	6484023
4	04ES-19-01-02	Dunite	507690	6481699
5	04ES-08-01-01	Dunite	508347	6481480
6	04ES-10-05-01	Dunite	507506	6484333
7	04ES-03-02-01	Dunite	508380	6481497
8	04ES-10-06-01	Wehrlite	507216	6484294
9	04ES-11-03-03	Wehrlite	506702	6484508
10	04ES-15-01-05	Wehrlite	511172	6481538
11	04ES-16-05-01	Wehrlite	511636	6481374
12	04ES-06-06-01	Olivine clinopyroxenite	507735	6481705
13	04ES-01-04-01	Olivine clinopyroxenite	509390	6481403
14	05ES-05-01-01	Olivine clinopyroxenite	506839	6483982
15	DDH04-47-7-49	Hornblende clinopyroxenite	506268	6482843
16	DDH05-84-19-104	Hornblende clinopyroxenite	505996	6482358

Number: refers to sample locations on Figure 1. Easting and Northing: UTM coordinates projected in NAD83, Zone 9.